JPE 9-3-5

Fault Diagnosis of Three-Phase PWM Inverters Using Wavelet and SVM

Dong-Eok Kim* and Dong-Choon Lee†

†*Dept. of Electrical Eng., Yeungnam University, Gyeonsan, Korea

ABSTRACT

In this paper, a diagnosis method for switch open-circuit faults in three-phase PWM inverters is proposed, which employs support vector machine (SVM) as classifying method. At first, a discrete wavelet transform (DWT) is used to detect a discontinuity of currents due to the fault, and then the features for fault diagnosis are extracted. Next, these features are employed as inputs for the SVM training. After training, the SVM produces an optimized boundary which is used identifying the fault. Finally, the fault classification is performed online with instantaneous features. The experimental results have verified the validity of the proposed estimation algorithm.

Keywords: Fault diagnosis, PWM inverters, Wavelet transform, Support vector machine

1. Introduction

Three-phase PWM inverters have been applied to industrial applications such as motor drives, power supplies, power quality conditioners, etc. The design and control techniques for PWM inverters have matured in commercial products as a result of efforts to enhance their performance. Despite well-developed designs and control algorithms, unexpected faults have often deteriorated the total reliability of the system. However, inverter fault diagnosis techniques have been paid little attention.

In induction motor drives, fault detection methods for winding insulation deterioration, rotor bar breakage, bearing damage, rotor eccentricity, etc. have been researched [1]-[4]. On the other hand, techniques for diagnosing inverter faults have been proposed in [5]-[7], where switch open-circuits and short-circuits, DC-link capacitor faults, line-to-earth faults, etc are categorized. Apart from the capacitor fault, the switch fault occurs most frequently. The switch short-circuit fault, which is the most frequent in switch-type faults, usually results in a shut-down mode for system protection. The switch open-circuit fault occurs due to frequent thermal cycling and gating driver failures. The switch open-circuit produces a dc-offset which may cause thermal damage in the opposite switch of the same leg and further gives the secondary faults to loads such that the motor bearing may be damaged due to torque pulsations or high currents may flow into the LC filters of UPS systems and the transformers. This paper focuses on the diagnosis of the switch open-circuit faults.

For detection of open-circuit faults, the inverter output voltage can be utilized [6]. However, this method requires additional voltage sensors even though its detection is fast. Most commonly, the current signal instead of the voltage is used for detection of switch open-circuit faults [8]-[10]. In [8], a fault diagnosis technique using a neural network was proposed, which includes a training process with the seven

Manuscript received Nov. 22. 2008; revised March 18, 2009
†Corresponding Author: dclee@yu.ac.kr
Tel: +82-53-810-2582, Fax: +82-53-810-4767, Yeungnam Univ.
*Dept. of Electrical Eng., Yeungnam Univ., Gyeonsan, Korea.

fault patterns according to the average of the Concordia current vector trajectory. This method gives a correct result, but its performance is not guaranteed in transient states. In addition, a technique using the current trajectory and the instantaneous frequency analysis was proposed [9], where the instantaneous frequency analysis cannot discriminate which switch is in fault, and a correct diagnosis is not guaranteed in transient states. In [10], the fault detection is performed by the ratio of the DC and the fundamental components of phase currents. However, in the case of applied vector control strategy, this method might generate a wrong fault flag since distorted sine waveforms are produced, which means the average in a cycle is positive or negative, when re-generating or braking modes occur due to sudden speed reference change. In [11], a fault diagnosis method using a neural network for multi-level inverters was introduced, in which the training of the neural network uses coefficients of the FFT (Fast Fourier Transform) analysis of output voltages. In this method, output voltage information for one full cycle is needed for FFT analysis.

In this paper, a new fault diagnosis technique that applies a DWT (Discrete Wavelet Transform) and a pattern recognition algorithm called a SVM (Support Vector Machine) is proposed. The instant when a fault occurs is detected with the DWT, and then the faulty switch is identified using the SVM. In the proposed scheme, fault detection and identification is performed in less than a half cycle. Whereas the current trajectory or artificial neural network techniques which use average current vectors need at least one cycle of current information, considering transient states. The effectiveness of the proposed diagnosis scheme has been verified by experimental results.

2. Open-Circuit Faults of Inverter Switches

Fig. 1 shows the typical three-phase PWM inverters. The switches of a leg are postulated ideal and operating without a dead-time. Fig. 2 shows the operating modes of switches at the normal condition (a-n, b-n) and the fault condition (a-f, b-f). Fig. 2(a) shows one case where the current-polarity is positive and (b) is the other case. First, if the upper switch of a leg, for example, switch S1 of leg A, is in fault, the corresponding phase voltage is decided by the polarity of current-flow and the switching pattern of switch S2. Leg A is connected to positive dc-bus by the upper by-pass diode D1 as shown in Fig 1. In this case, the current is rapidly decreased to zero through diode D2 and kept at zero, and other two phase currents are in opposite phase as shown in Fig. 3. Then, if upper switch S1 of leg A is in fault as the negative-current flows, the switch fault does not affect the current flow since the current flows through diode D1 as shown in Fig. 3. On the contrary, if

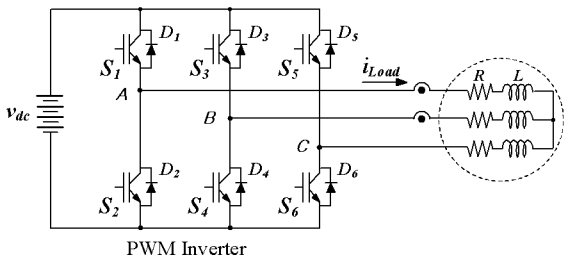

Fig. 1. PWM Inverter.

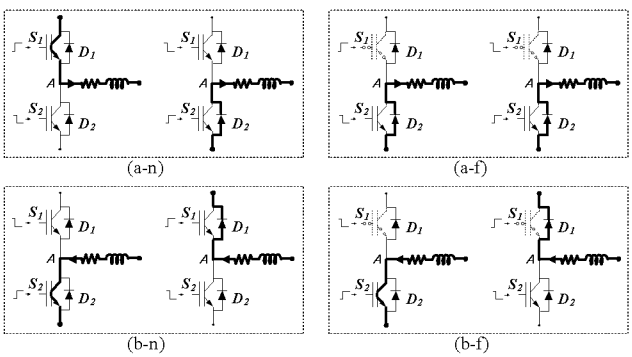

Fig. 2. Current flows (a) Positive (b) Negative: (a-n, b-n) normal condition and (a-f, b-f) upper switch fault condition.

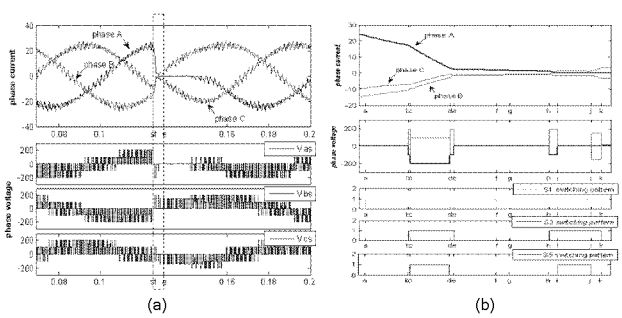

Fig. 3. S1 open-fault (a) phase current and voltage waveforms (b) zoom-in of (a) and gate signal S1, S3, S5.

switch S2 of leg A is in fault, a fault phenomenon occurs at the negative-polarity of the current flow since leg A is connected to the negative DC-bus by the bottom by-pass diode D2. Consequently, if a switch open-circuit fault arises, the current is kept in zero for about a half-period, so that the current includes DC-offset components.

3. Discrete Wavelet Transform

DWT is a efficient tool applied not only to the field of such signal processing as noise elimination and image compression but also in the analysis of disturbances in waveforms owing to its capability to detect discontinuities quickly [12].

In the multi resolution analysis (MRA) which is a method of DWTs, a multi resolution approximation is characterized by the scaling function ϕ that generates an orthogonal basis of each space $\mathbf{V}_j$. For example, the approximation of f at the scale 2^j and 2^{j-1} are equal to their orthogonal projection on $\mathbf{V}_j$ and $\mathbf{V}_{j-1}$, respectively, where $\mathbf{V}_j$ is included in $\mathbf{V}_{j-1}$. In the same way, the wavelet function ψ carries the detail components required to increase the resolution of a signal approximation, where ψ is an orthogonal basis of $\mathbf{W}_j$ which is the orthogonal complement of $\mathbf{V}_j$ in $\mathbf{V}_{j-1}$ as $\mathbf{V}_{j-1} = \mathbf{V}_j \oplus \mathbf{W}_j$.

The orthogonal projection of f on $\mathbf{V}_{j-1}$ can be decomposed as the sum of orthogonal projection on $\mathbf{V}_j$ and $\mathbf{W}_j$ as

$$P_{\mathbf{V}_{j-1}} f = P_{\mathbf{V}_j} f + P_{\mathbf{W}_j} f \tag{1}$$

where,

$$P_{\mathbf{V}_j} f = \sum_{n=-\infty}^{+\infty} < f, \phi_{j,n} > \phi_{j,n}\ ,\ P_{\mathbf{W}_j} f = \sum_{n=-\infty}^{+\infty} < f, \psi_{j,n} > \psi_{j,n}$$

$$\phi_{j,n}(t) = 2^{-j/2}\phi\left(2^{-j}t - n\right),\quad \psi_{j,n}(t) = 2^{-j/2}\psi\left(2^{-j}t - n\right).$$

The $P_{\mathbf{W}_j} f$ and the compliment of $P_{\mathbf{V}_j} f$, provide the details of f, which appear at the scale 2^{j-1} and disappear at the coarser scale 2^j. Therefore, $\mathbf{W}_j$ is called a detail space or wavelet space. Any $\phi_{j+1,p} \in \mathbf{V}_{j+1} \subset \mathbf{V}_j$ and $\psi_{j+1,p} \in \mathbf{W}_{j+1} \subset \mathbf{V}_j$ can be decomposed in the orthogonal basis $\{\phi_{j,n}\}_{n\in Z}$ of $\mathbf{V}_j$ as

$$\phi_{j+1,p} = \sum_{n=-\infty}^{+\infty} < \phi_{j+1,p}, \phi_{j,n} > \phi_{j,n} = \sum_{n=-\infty}^{+\infty} h[n-2p]\phi_{j,n} \tag{2}$$

$$\psi_{j+1,p} = \sum_{n=-\infty}^{+\infty} < \psi_{j+1,p}, \phi_{j,n} > \phi_{j,n} = \sum_{n=-\infty}^{+\infty} g[n-2p]\phi_{j,n} \tag{3}$$

Taking the inner product with f on each side gives

$$a_{j+1}[p] = \sum_{n=-\infty}^{+\infty} h[n-2p]a_j[n] = a_j * h[-2p] \tag{4}$$

$$d_{j+1}[p] = \sum_{n=-\infty}^{+\infty} g[n-2p]a_j[n] = a_j * g[-2p] \tag{5}$$

where " * " means a convolution.

The process of (4) and (5) is shown in Fig. 4. To sum up, the DWT is to project a function with filters from a higher resolution domain to a lower one sequentially as shown in Fig. 4. In Fig. 4, h is a kind of low-pass filter and g is a high-pass filter, a_j is an approximation coefficient and d_j is a detail coefficient or a wavelet coefficient which results from mapping f to wavelet spaces.

4. Support Vector Machine

The SVM is a classifying method used often for pattern recognition applications like face recognition as well as for data mining [13].

The objective of the SVM is to find out a separating boundary with a maximum distance between two classes composed of training data, where one class is a white circle group and the other is a black circle group, as shown in Fig. 5. It can be achieved by solving the following dual problems [14].

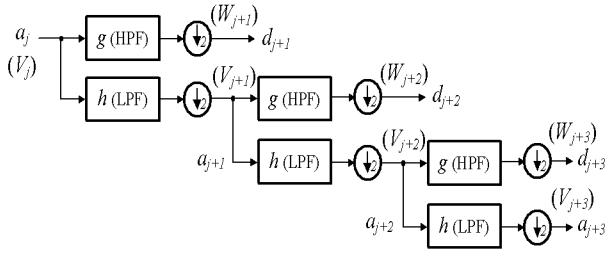

Fig. 4. Filter bank structure for DWT. (3-stage, 3-channel structure)

$$\text{Maximize: } W(\alpha)=\sum_{i=1}^{N}\alpha_i-\frac{1}{2}\sum_{i=1}^{N}\sum_{j=1}^{N}\alpha_i\alpha_j y_i y_j K(\mathbf{x}_i,\mathbf{x}_j) \quad (6)$$

$$\text{Subject to: } \sum_{i=1}^{N}\alpha_i y_i=0,\ 0\le\alpha_i\le C,\ \forall i=(1,2,...,N) \quad (7)$$

$$K(\mathbf{x},\mathbf{x}')=(<\mathbf{x},\mathbf{x}'>+1)^d \quad (8)$$

where α_i is a Lagrange multiplier, $(\mathbf{x}_i, y_i)$ is a training data set in which $\mathbf{x}_i$ is input data and y_i is output data. C is a constant for a trade-off between the performance and the generalization, and $K(\mathbf{x},\mathbf{x}')$ is a polynomial kernel function that performs the non-linear mapping into the feature space.

Solving (6) with the constraints of (7), the Lagrange multipliers $\{\alpha_i\}_{i=1}^{N}$ are determined and a separating function is obtained as

$$f(x)=sign\left(\sum_{i=1}^{N_{SV}}\alpha_i y_i K(\mathbf{x}_i,\mathbf{x})+b\right) \quad (9)$$

where b is a bias term as

$$b=-\frac{1}{2}\sum_{i=1}^{N}\alpha_i y_i\left[K(\mathbf{x}_i,\mathbf{x}_r)+K(\mathbf{x}_i,\mathbf{x}_s)\right]$$

and N_{SV} is the number of support vectors, which are $\mathbf{x}_i$ with non-zero α_i.

One advantage of the SVM is that it can provide a globally optimized separating boundary with only a few support vectors among lots of training data, unlike other learning machines that have a risk of local minima.

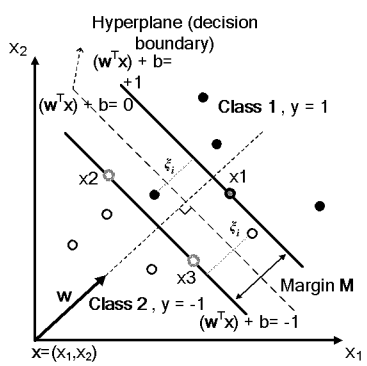

Fig. 5. Classification of two classes with maximum margin.

In addition, the SVM can be applied for function estimation such as wind speed estimation or current estimation [15-16], in which SVM is called SVR(Support Vector Regression).

5. Fault Diagnosis of Inverter Switch

Current signals are used for the inverter switch open-circuit fault diagnosis. However, a sudden change of current amplitude by transient states is one obstacle in performing fault diagnosis. Therefore, a process normalizing the amplitude of the current to a constant value is needed. The current can be normalized as

$$i_{a,b,c\_nml}=\frac{i_{a,b,c}}{\sqrt{i_{ds}^2+i_{qs}^2}} \quad (10)$$

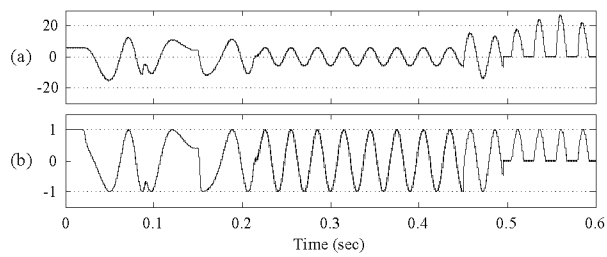

Fig. 6. Current waveforms. (a) Original (b) Normalized

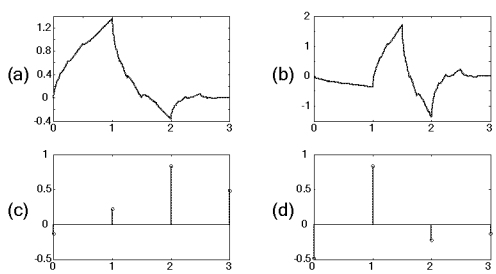

Fig. 7. Daubechies 2. (a) Scaling (b) Wavelet (c) Low-pass filter coefficients (d) High-pass filter coefficients

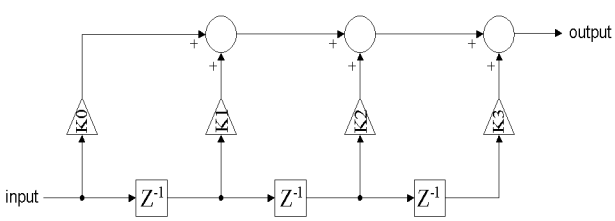

Fig. 8. FIR filter structure applying db2.

where, $i_{a,b,c}$ are original phase currents, i_{a,b,c_nml} are normalized phase currents, i_{ds} and i_{qs} are the d- and q-axis currents in a stationary reference frame.

Fig. 6 shows the original current waveform and the normalized current waveform. In Fig. 6, the fault occurred at around 0.5[s] and the magnitude of current rapidly diminished to zero at that point. However, the amplitude of the normalized current signal was not affected by load conditions before 0.5[s].

Then, the normalized current waveforms are transformed into frequency domain by the DWT. The DWT is realized easily with several FIR (Finite Impulse Response) filters which are achieved by applying the db2 (daubechies2) scale and wavelet. The corresponding scale, wavelet, and filter coefficients are shown in Fig. 7. The horizontal scale of wavelet is 2N-1, where N is the order of wavelet (N of db2 is 2). Also, the structure of FIR filters obtained by applying db2 is shown in Fig. 8, where the filter coefficients K0, K1, K2 and K3 are listed in Table 1.

Fig. 9 shows the original current waveforms, normalized waveforms, 1st and 2nd detail coefficients obtained by applying the db2 wavelet to the normalized of (a), (d), and (g), respectively, from the top. Here, the 1st and 2nd detail coefficients correspond to d_{j+1} and d_{j+2} in Fig. 4. The switching frequency is 5[kHz] and the sampling frequencies of the FIR filters at the first and second stages are 10[kHz] and 5[kHz], respectively. In fact, a clear discontinuity never occurs in the faulted phase current waveform except for a fault instant, but the discontinuities come about in the other phase currents while the faulted-phase current is kept at zero as shown in Fig. 9. If the current signal has a discontinuous condition, the detail coefficient has a sudden increased amplitude and narrowed wavelength for a short time at the discontinuous point. Hence, the discontinuity can be detected easily with a certain threshold pre-determined.

However, it cannot classify which switch is in fault not only because the discontinuity occurs in both current waveforms of a faulty phase and the other phases, but also because the discontinuity may be produced due to disturbances or abrupt reference changes. Therefore, an additional technique for classifying the fault is required, which is to count the zero current samples. Considering sensor offsets, the number of current samples placed within a certain range is counted instead. In this work, the range is chosen from -0.2 to 0.2, within which the samples are called zero current samples for convenience.

Fig. 10 shows normalized current waveforms and the number of current samples within a certain range under the normal and fault conditions. It is easily noticed that the number of zero current samples is different according to conditions. In order to find an optimal decision boundary between the normal and fault conditions as shown in Fig, 4, a learning machine SVM is used.

Fig. 11 shows the current waveforms of a faulty phase with the upper switch broken. Fig. 11(a)-(c) show the cases when the upper-switch is broken when the positive current flows, where (a) has a high descent and positive average value and (b) has a high descent as well, but the average is almost zero, and the descent in (c) is very low and the average is negative. (d) and (e) are the cases in which the switch brakes when the negative current flows, where the both descent of (d) and (e) are nearly zero and the average values are definitely negative. Therefore, once a fault phase is discriminated by the SVM, the fault switch is easily classified with the other SVM as well, of which

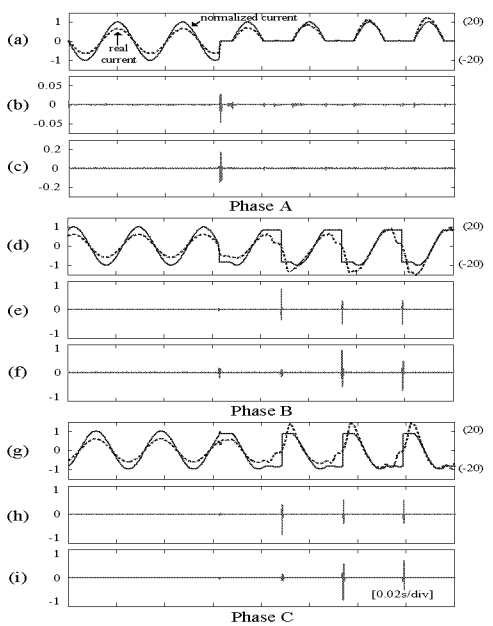

Fig. 9. Results of DWT. (a),(d),(g) Original and normalized current waveform. (b),(e),(h) 1st detail coefficient (2.5~5[kHz]). (c),(f),(i) 2nd detail coefficient (1.25~2.5[kHz])

features are the average of past half-cycle and the tilt during a quarter cycle from the fault instant detected by DWT as shown in Fig. 11.

Fig. 12 shows how to extract features for the proposed fault diagnosis method from the normalized current waveform, where SVM1 and SVM2 are used to classify the faulty phase and the faulty switch, respectively. First, the count of zero current samples for the previous half and next quarter cycles at the detection point are chosen as the features which are the input data of SVM1. The features are each numbers of filled-squares and circles that are placed within the band width in Fig. 12. Then, the sum of samples (sum of i[k] from k=-n_i to k=0 in Fig. 12) during the previous half cycle and the variation of samples ((i[0] – i[n_j]) in Fig. 12) during the next quarter cycle are chosen as the inputs of SVM2, where i[0] is the current value at the detection point of the discontinuity and i[n_j] is the one at the next quarter cycle past the detection point. Also, the n_i and n_j are total numbers of the current samples during the previous half and the next quarter cycles, respectively, which are constant without reference to the frequency. The features explained above are used for training data of SVMs off-line and for running inputs of SVMs on-line.

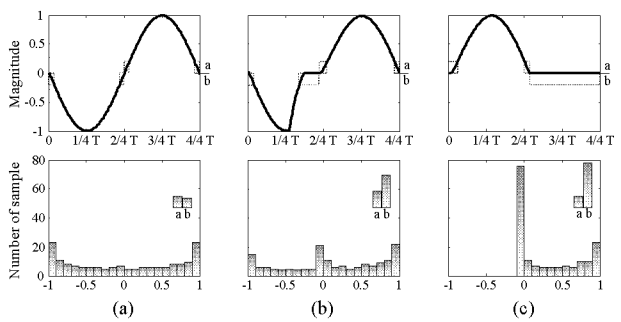

Fig. 10. Current waveforms and histograms in (a) Normal condition (b),(c) Fault conditions.

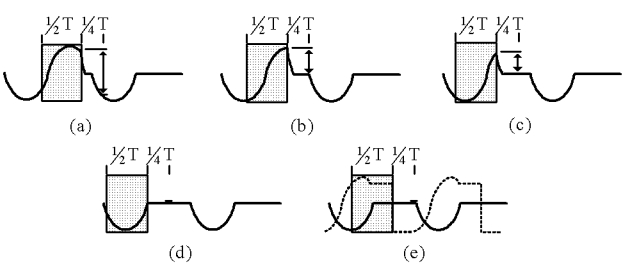

Fig. 11. Current waveforms in fault (a)-(c): With positive current flow (d),(e): With negative current flow.

Off-line training of the SVM using these features determines the support vectors, Lagrange multipliers, constant C, and bias term b. With running input data, a fault decision can be made by using (4).

Fig. 13 shows a fault diagnosis structure with a separating function f(x) of SVMs, where SVM1 training is performed with features obtained from all three phase currents since a separating function obtained from the training is applied to all three phases. The output of SVM2 is activated only when the output of SVM1 is '+1' which means a fault condition.

A flow chart of fault diagnosis, in summary, is shown in Fig. 14. At first, the normalization of phase currents is performed. Then, a discontinuity in current waveforms is detected with the DWT. Next, the features for fault diagnosis are selected and collected under various conditions, and then SVM training is performed off-line with the features. Finally, the fault is classified by the separating function on-line.

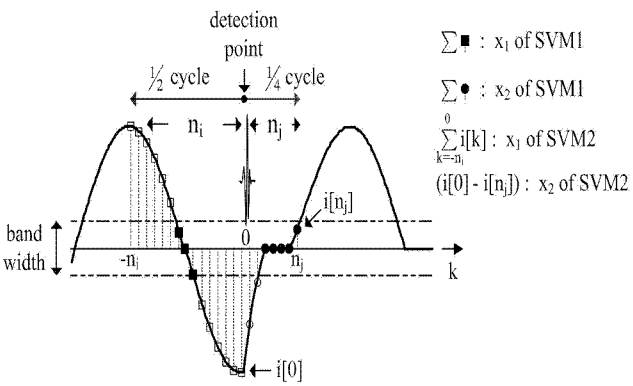

Fig. 12. Feature extraction from the normalized current waveform.

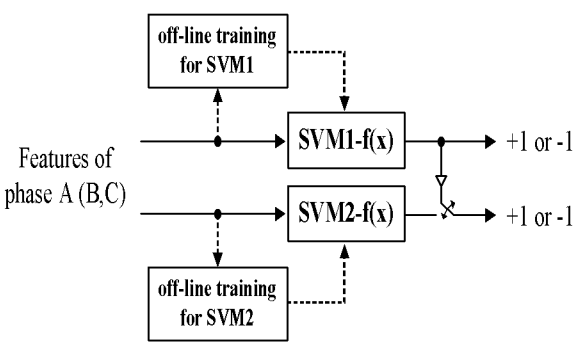

Fig. 13. Fault diagnosis structure with separating functions.

6. Experimental Results

The experiment has been performed to verify the proposed method. The DSP board with a TMS320VC33 is used as a main controller. The inverter switching frequency is 5[kHz], the AC source voltage is 220[Vrms] and 60[Hz], and three-phase diode rectifiers are used for the dc-source of the inverter, of which the dc-link capacitance is 1,950[uF]. The squirrel-cage induction motor is rated at 3[kW], which is controlled in the indirect vector control mode.

First, in order to confirm that the proposed method does not make any wrong fault flags in harsh conditions (non-fault conditions), the fault flag was observed in abrupt variations of frequency and amplitude.

Fig. 15-17 show phase current waveforms for RL loads (5[Ω], 7[mH]) and fault flags. The flags of '-1' and '+1' represent normal and fault conditions, respectively.

Fig. 15 shows the case where the amplitude of currents is controlled constantly and the frequency of currents is changed several times abruptly. The upper switch of the A-phase has been open-circuited at a certain point, and then the only fault flag of the A-phase shifted from '-1' to '+1'.

In the case of Fig. 16, the amplitude of currents is changed several times abruptly and the frequency of currents is fixed. The fault condition is the same as in the case of Fig. 15. Likewise, unless the fault condition is produced, the fault flag is not generated.

Fig. 17 shows the case where both the amplitude and the frequency changed sinusoidally. As the fault flag of

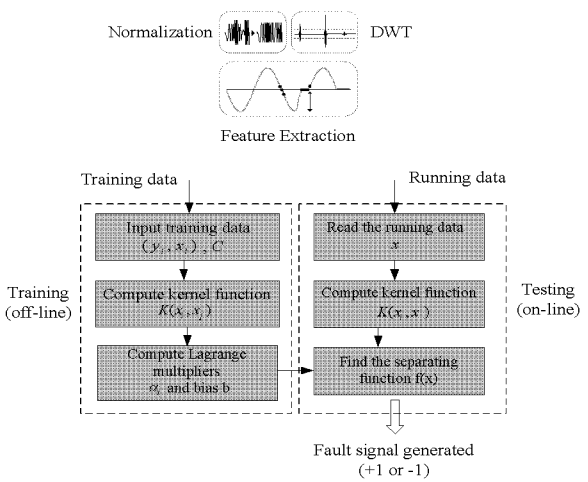

Fig. 14. Flow chart of the proposed fault diagnosis.

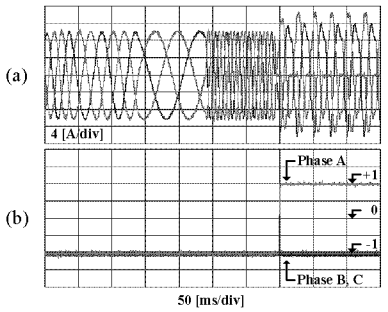

Fig. 15. Phase current waveforms and fault flags (-1: normal , +1: fault) in case of RL load. (a) Inverter output fre quency variation. (b) Fault flags.

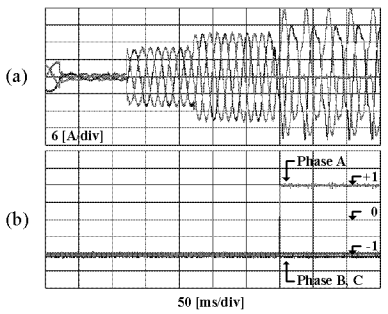

Fig. 16. Phase current waveforms and fault flags (-1: normal , +1: fault) in case of RL load. (a) Amplitude variation. (b) Fault flags.

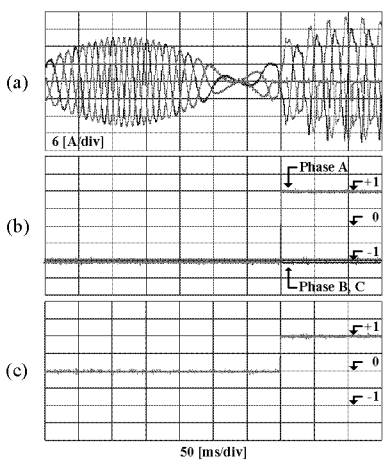

Fig. 17. Phase current waveforms and fault flags (-1: normal , +1: fault) in case of RL load. (a) Both variations of frequency and amplitude (ref: f=60sin1.5πt, I_{mag}=15sin1.5πt). (b) Fault flags for each phase. (c) Fault flags for switch. (-1: bottom switch fault, +1: upper switch fault).

the A-phase is shifted to '+1', the flag for faulty switch identification is changed to '+1', which means the upper switch fault (of the flag for fault-switch, '-1' means the bottom switch fault and '+1' means the upper switch fault). Fig. 18 shows real current waveforms and normalized current waveforms.

Next, the experiments are performed for vector-controlled IM drives. Fig. 19 shows the case of induction motor drives in which the speed profile changes in ramp, which gives a correct diagnosis result (no fault flag generated).

Fig. 20 shows the fault flags when there is a fault in the upper or bottom switch of the A-phase. It is noticed that the flag signal is generated correctly within a quarter-period.

Fig. 21 shows the diagnosis results for fault-phase and fault-switch. As the upper switch of A-phase is open-faulted, both the fault flag for phase-A and the flag for fault-switch identification are shifted to '+1'. As the bottom switch of the A-phase is open-faulted, the fault flag for phase-A is changed to '+1' as well, but the flag for fault-switch identification is shifted to '-1'.

7. Conclusions

In this paper, a diagnosis scheme for inverter switch open-circuit faults has been proposed. The discontinuity due to faults is detected with the DWT. While the faulty phase and the faulty switch was classified with the separating function of the SVM, which needs a little effort with off-line training. This proposed method can detect and classify which switch is in fault in less than a half period, and it is robust in the transient state. Experimental results have verified the effectiveness of the proposed diagnosis algorithm.

Appendix

Table 1 Filter coefficients

	Low-pass filter	High-pass filter
K0	-0.129409522550917	-0.482962913144691
K1	0.224143868041857	0.836516303737465
K2	0.836516303737465	-0.224143868041857
K3	0.482962913144691	-0.129409522550917

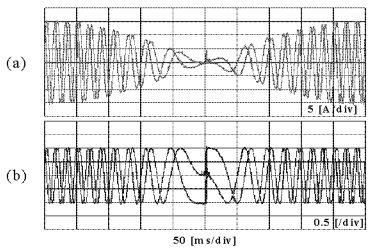

Fig. 18. Current waveforms. (a) Real current waveforms (b) Normalized current waveforms

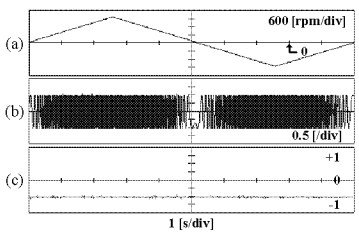

Fig. 19. Normal conditions operating with induction motor. (a) Speed (b) Normalized current waveform (c) Fault flag.

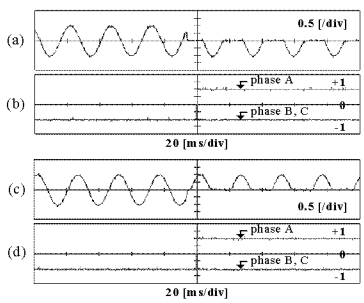

Fig. 20. Fault condition operating induction motor 1. Upper switch fault: (a) Normalized current waveform of phase-A (b) Fault flags for each phase. 2. Bottom switch fault: (c) Normalized current waveform of phase-A. (d) Fault flags for each phase.

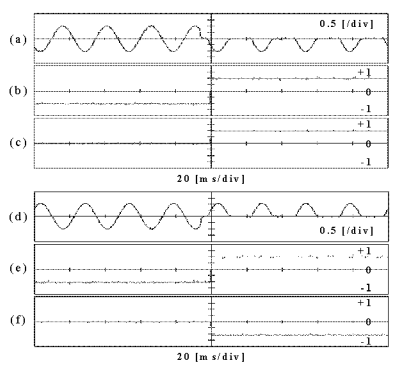

Fig. 21. Fault flags for phase A. 1. Upper switch fault: (a) Normalized current waveform of phase-A. (b) Fault flags for phase-A. (c) Fault flags for switch. 2. Bottom switch fault. (d) Normalized current waveform of phase-A. (e) Fault flags for phase-A. (f) Fault flags for switch.

Acknowledgement

This research was supported by the Yeungnam University research grants in 2007.

References

[1] M. S. Ballal, H. M. Suryawanshi, and M. K. Mishra, "Detection of incipient faults in induction motors using FIS, ANN and ANFIS techniques," *Journal of Power Electronics*, Vol. 8, No. 2, pp. 181-191, April 2008.

[2] M. E. H. Benbouzid, and G. B. Kliman, "What stator current processing-based technique to use for induction motor rotor faults diagnosis?," *IEEE Trans. Energy Conv.*, Vol. 18, No. 2, pp. 238-244, June 2003.

[3] N. H. Kim, "Rotor fault detection system for inverter driven induction motor using current signals and an Encoder," *Journal of Power Electronics*, Vol. 7, No. 4, pp. 271-277, Oct. 2007.

[4] X. Huang, T. G. Habetler, and R. G. Harley, "Detection of rotor eccentricity faults in a closed-loop drive-connected induction motor using an artificial neural network," *IEEE Trans. Power Electron.*, Vol. 22, No. 4, pp. 1552-1559, July 2007.

[5] A. Lahyani, P. Venet, G. Grellet, and P. J. Viverge, "Failure prediction of electrolytic capacitors during operation of a switchmode power supply," *IEEE Trans. Power Electron.*, Vol. 13, No. 6, pp. 1199-1207, Nov. 1998.

[6] D. Kastha and B. K. Bose, "Investigation of fault modes of voltage-fed inverter system for induction motor drive," *IEEE Trans. on Industry Applicat.*, Vol. 30, No. 1, pp. 1028-1038, July/August 1994.

[7] R. L. de Araujo Ribeiro, C. B. Jacobina, E. R. C. da Silva, and A. M. N. Lima, "Fault detection of open-switch damage in voltage-fed PWM motor drive systems," *IEEE Trans. Power Electron.*, Vol. 18, No.2, pp. 587-593, March 2003.

[8] D. Diallo, M. E. H. Benbouzid, D. Hamad, and X. Pierre, "Fault detection and diagnosis in an induction machine drive: a pattern recognition approach based on concordia stator mean current vector," *IEEE Trans. Energy Conv.*, Vol. 20, No. 3, pp. 512-519, Sept. 2005.

[9] R. Peuget, S. Courtine, and J. P. Rognon, "Fault detection and isolation on a PWM inverter by knowledge-based model," *IEEE Trans. Ind. Applicat.*, Vol. 34, No. 6, pp. 1318-1326, Nov./Dec. 1998.

[10] S. Abramik, W. Slezynski, J. Nieznanski, and H. Piquet, "A diagnostic method for on-line fault detection and localization in VSI-fed ac drives," *EPE Proc.*, France, CD-ROM paper, 2003.

[11] S. Khomfoi, and L. M. Tolbert, "Fault diagnosis system for a multilevel inverter using a neural network," *IEEE Trans. Power Electron.*, Vol. 22, No. 3, pp. 1062-1069, May 2007.

[12] S. Mallat, Wavelet tour of signal processing, Academic press, 2nd Ed, 2000.

[13] V. Kecman, Learning and Soft Computing, MIT Press, pp. 121-191, 2001.

[14] D. J. Sebald, and J. A. Bucklew, "Support vector machine techniques for nonlinear equalization," *IEEE Trans. Signal Process.*, Vol. 48, No. 11, pp. 3217-3226, Nov. 2000.

[15] A. G. Abo-Khalil and D.-C. Lee, "MPPT control of wind generation system based on estimated wind speed using SVR," *IEEE Trans. Ind. Electron.*, Vol. 55, No. 3, pp. 1489-1490, March 2008.

[16] D.-C. Lee and A. G. Abo-Khalil, "Optimal efficiency control of induction generators in wind energy conversion systems using support vector regression," *Journal of Power Electronics*, Vol. 8, No. 4, pp. 345-353, Oct. 2008.

Dong-Eok Kim received the B.S. and M.S. in Electrical Engineering from Yeungnam University, Gyeongbuk, Korea, in 2005 and 2008, respectively. He was an engineer with LG Philips LCD (LG Display) in 2005. Since 2008, he has been a research engineer in Electrical Technology Research Department, Institute of Information and Communication, Yeungnam University. His research interests are power converter control, motor control, power quality, and fault diagnosis.

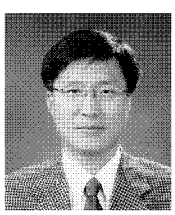

Dong-Choon Lee received the B.S., M.S., and Ph.D. degrees in Electrical Engineering from Seoul National University, Seoul, Korea, in 1985, 1987, and 1993, respectively. He was a Research Engineer with Daewoo Heavy Industry from 1987 to 1988. Since 1994, he has been a faculty member of the Dept. of Electrical Engineering, Yeungnam University, Gyeongbuk, Korea. As a Visiting Scholar, he joined Power Quality Laboratory, Texas A&M University, College Station in 1998, and Electrical Drive Center, University of Nottingham, U.K. in 2001, and Wisconsin Electric Machines & Power Electronic Consortium, University of Wisconsin, Madison in 2004. His research interests include ac machine drives, control of power converters, wind power generation, and power quality. Prof. Lee is currently a Publication Editor of the Journal of Power Electronics of the Korean Institute of Power Electronics.